




# Magnetron sputter deposition of Ta<sub>2</sub>O<sub>5</sub>-SiO<sub>2</sub> quantized nanolaminates

S. SCHWYN THÖNY,<sup>1,\*</sup> M. BÄRTSCHI,<sup>2</sup> M. BATZER,<sup>1</sup> M. BASELGIA,<sup>1</sup>  
S. WALDNER,<sup>1</sup> M. STEINECKE,<sup>3</sup> H. BADORRECK,<sup>3,4</sup>  
A. WIENKE,<sup>3,4</sup>  AND M. JUPÉ<sup>3,4</sup>

<sup>1</sup>Evatec AG, Hauptstrasse 1a, 9477 Trübbach, Switzerland

<sup>2</sup>RhySearch, Werdenbergstrasse 4, 9471 Buchs, Switzerland

<sup>3</sup>Laser Zentrum Hannover e.V., Optical Components Department, Holleritallee 8, 30419 Hannover, Germany

<sup>4</sup>Cluster of Excellence PhoenixD (Photonics, Optics, and Engineering innovation across Disciplines), Leibniz University Hannover, Welfengarten 1A, 30167 Hannover, Germany

\*[silvia.schwyn-thoeny@evatecnet.com](mailto:silvia.schwyn-thoeny@evatecnet.com)

**Abstract:** Quantized nanolaminates are a type of optical metamaterials, which were discovered only recently. Their feasibility was demonstrated by atomic layer deposition and ion beam sputtering so far. In this paper, we will report on the successful magnetron sputter deposition of quantized nanolaminates based on Ta<sub>2</sub>O<sub>5</sub>-SiO<sub>2</sub>. We will describe the deposition process, show results and material characterization of films deposited in a very wide parameter range. Furthermore, we will show how quantized nanolaminates deposited by magnetron sputtering were used in optical interference coatings such as antireflection and mirror coatings.

© 2023 Optica Publishing Group under the terms of the [Optica Open Access Publishing Agreement](#)

## 1. Introduction

Optical coatings are a basic requirement for the efficient function of optical components. Almost all optical components derive a large part of their spectral properties from the quality of the interference filters applied to the optics. Even though the manufacturing concepts and the complexity of the designs have increased in recent years, most coatings are still based on established oxide materials, which are combined in a layer system to form an interference filter. As the demands on the filters continue to increase, there is also a growing need for alternative materials with better performance. Metamaterials are increasingly being considered, in which the functionality is not based exclusively on the material properties themselves, but new physical properties are achieved through the artificially engineered structural modification of the materials.

Quantized nanolaminates (QNL), which were first proposed in 2017 [1,2] belong to this new class of engineered materials. In QNLs, sub-nanometer thin dielectric layers of high and low refractive index materials are stacked. The limited structure size leads to quantization effects, which enable to shift not only the material's refractive index but also the band gap of the material independent of each other. This is in contrast to classical dielectric materials, in which the refractive index and the energy of the absorption edge are fundamentally linked [3].

Previous work aiming at decoupling refractive index and band gap focused on self-organizing structures, which acquire their functionality through localized or unlocalized porous structures and reduce the refractive index [4]. One approach for their preparation is glancing angle deposition [5–9], in which a columnar film structure is formed, which reduces the effective refractive index. Interference effects will occur between bulk-like layers and layers with columnar structure of one and the same material. Another approach uses self-organizing structures achieved by ion etching [10–13], which also reduces the effective refractive index. The reduction of the index is especially beneficial in the case of SiO<sub>2</sub>, since lower indices can be achieved than available by standard materials opening up a wide field of applications.

In the above approaches, only the optical property of refractive index is manipulated, whereas the energy gap defined by electronic properties remains unchanged. In this paper, however, structures will be shown, which selectively couple back to the electronic properties of the material. Similar approaches are currently only available in multi quantum well (MQW) structures in optoelectronics where the optical emission wavelength and power is adjusted by the state densities of the electrons via confinement. Even though the MQW concept is based on crystalline structures, Willemsen et al. [2,14] have shown that the crystalline structure is by no means the precondition for the occurrence of quantum effects and that they can also be observed in amorphous dielectric materials.

In the practical application the shift of the energy gap in QNL can be adjusted by the physical thickness of the high index material, whereas the thickness ratio of the high and low index materials determines the effective refractive index of the QNL. Thus, a two-dimensional parameter field is obtained in which the energy gap and the refractive index can be adjusted separately from each other in a defined range.

The objective for the application of such quantizing metamaterials is to extend the useful range of specific materials below the band gap of the high index material of the QNL. As an example, in the UV range the band gap of Ta<sub>2</sub>O<sub>5</sub> can be pushed towards shorter wavelengths and so provide an alternative to the use of HfO<sub>2</sub>. This is desirable since hafnium targets are expensive and because HfO<sub>2</sub> tends to form polycrystalline grain boundaries while growing, which can cause losses by scattering of light.

The QNL effect has been demonstrated experimentally for atomic layer deposition (ALD) and ion beam sputtering (IBS) [15] coatings, but not until now for magnetron sputtering. Although both of former methods lead to good results, they do have drawbacks with regards to volume production. ALD has low growth rates since only one atomic layer is deposited per coating cycle, whereas, in IBS a zone target needs to be mechanically translated from one material of the nanolaminate to the other also limiting the deposition rate.

In contrast, the turntable configuration of the Evatec Clusterline 200BPM magnetron sputter system is ideally suited to the deposition of QNL, since both materials can be deposited in one table rotation. We will show in this paper how the process is implemented for the material combination Ta<sub>2</sub>O<sub>5</sub> and SiO<sub>2</sub> in this magnetron sputter deposition system and we will demonstrate that the quantizing effect is observed as predicted. Furthermore, we will take this result and show that an antireflection coating at 280 nm and a mirror at 355 nm can be manufactured consisting of the Ta<sub>2</sub>O<sub>5</sub>-SiO<sub>2</sub> QNL and SiO<sub>2</sub>.

## 2. Theory

To understand why QNL should be used, one can consider the general classical mode of action for interference filters. Optical interference coatings such as anti-reflection, mirror or filter coatings are based on stacks of materials with at least two different refractive indices,  $n$  in alternating layers. The resulting effect of the interference is correlated with the difference in refractive index between the materials. As a consequence, layer stacks with high refractive index difference require a smaller number of individual layers in the optical design and thus less overall thickness than stacks with a low difference in index. In addition to the refractive index the materials have to fulfill another requirement, namely a high transparency with negligible losses in the wavelength range of interest. The absorption of an optical material is mainly determined by its band gap energy, which determines the upper limit for the energy of transmitted photons.

However, in dielectric materials the refractive index and the energy of the absorption gap are fundamentally linked [3]. Materials with high refractive index have their absorption gap at a low photon energy while low refractive index materials have the absorption edge at high photon energies.

Figure 1 shows a schematic diagram of the periodic structure of a quantized nanolaminate. The theory of the quantized nanolaminates is based on the combination of the quantum mechanical and the classical approach. A canonic solution is described in [16,17]. The optical properties of the QNL can be calculated by the effective medium theory. Actually, the QNL are defined by the upper Wiener limit [18,19]. The effective refractive index of the resulting meta-material  $n_{eff}$  is defined by the ratio of high and low refracting materials and can be calculated by applying the effective medium theory.  $f$  denotes the volume ratio between high and low refracting materials [20]:

$$n_{eff}^2(\lambda) = fn_{high}^2(\lambda) + (1-f)n_{low}^2(\lambda) \quad (1)$$

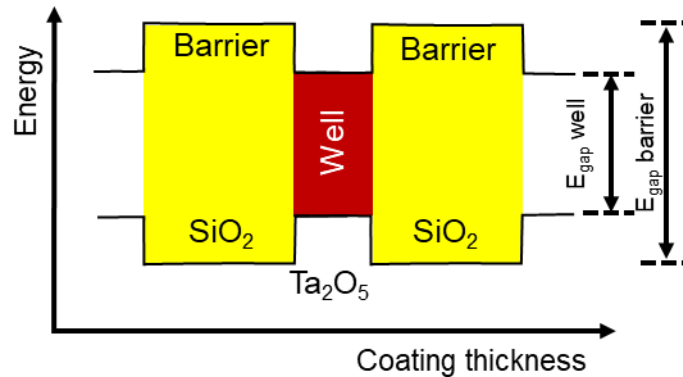
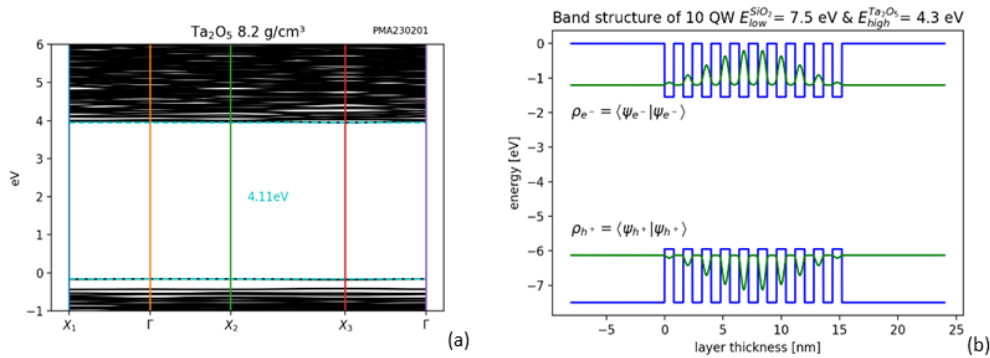


Fig. 1. Periodic structure of high and low band gap areas, which limit the electron mobility.

The thickness of the individual high and low refractive index layers in the QNL can be calculated by multiplying the total thickness per rotation with the volume ratio  $f$  of the high index material, respectively  $(1-f)$  for the low index material. This simple formula shows that the refractive index of the QNL metamaterial is always between the values of the high and low refractive index materials and defines the physical refractive index limits of the metamaterial. The actual gain of the material comes from the displacement of the band gap. First of all, a brief look at the electronic material properties is necessary. As already mentioned, optical coatings mostly produce amorphous or polycrystalline materials whose band structure is not clearly defined. Thus, the band gap itself can be regarded as a depletion zone of states and the densities between bound and free states are so low that they can be neglected [21]. Thus, the potential wall, which is necessary for the quantization is clearly defined. Figure 2(a) shows the band structure of amorphous  $Ta_2O_5$ , according to the density functional theory (DFT) calculation using hybrid functionals by MedeA/VASP [22,23]. Obviously, the gaps are clearly defined, but there are no bands for the bound and the quasi-free states. Actually, the gap is covered by ensembles of states which are related to the random long-distance order of the atoms.

The situation is more complicated with respect to the mobility of the quasi-free electrons. In crystals the mobility is connected to the curvature of the bands. This is not applicable to amorphous solids; therefore, the effective mass of holes and electrons have to be fitted.

Independent of the band structure the mobility of the carrier can be limited by an electronic confinement. In the case of the QNLs, a periodic structure of high and low band gap materials (blue solid line) is generated in the growth direction. Figure 2(b) shows the probability of electronic states as a green solid line for an example of a QNL consisting of 10 quantum wells. The probability is concentrated towards the center of the QNL in the high index material  $Ta_2O_5$ . With respect to the correlation between band gap and refractive index, the low index material will act as a barrier whereas the high index material acts as the quantum well, as shown in Fig. 1. As



**Fig. 2.** Electronic structure of amorphous  $\text{Ta}_2\text{O}_5$  with a gap of  $E_{\text{Gap}}^{\text{Ta}_2\text{O}_5} = 4.11 \text{ eV}$  (a) and band structure of QNL with 10 quantum wells of  $\text{SiO}_2$  and  $\text{Ta}_2\text{O}_5$  (b).

already indicated, the reduction of the layer thickness leads to new states which can be calculated by solving the Schrödinger equation. A closed analytic solution can be given only for a few potentials, like the infinite quantum well or the parabolic form [16]. For this work we assumed finite quantum wells and a periodic sequence. The energy levels in the singular quantum well can be obtained numerically via the algorithms already quoted [2,15]. However, this solution neglects the interaction between the quantum wells, so for this work a matrix solution of the discretized Schrödinger equation was used, adapted to the boundary conditions. For the solution we refer here to the literature [17].

Thus, the thickness of the quantum well will determine the shift in band gap, whereas the thickness ratio of high to low band gap material will determine the refractive index. Thus, the novel concept of so-called quantizing nanolaminates (QNLs) allows for independent adjustment of the optical band gap and refractive index. To achieve the desired quantization, the thickness of each quantum well layer should be smaller than 2 nm, with barrier thickness in the same range. As an example, for a thickness of 2 nm the offset is 0.08 eV, which is very small compared to about 4.1 eV of band gap energy and represents a shift of only 5 nm. To achieve a shift, which is of practical use, the quantum well should be chosen much smaller, since the energetic offset is proportional to  $d_{\text{well}}^{-2}$  in first order. Since this is a simple potential consideration, even non-closed atomic layers can lead to a suitable periodic potential. The thickness of the barrier influences the refractive index of the QNL (see Eq. (1)). On the other hand, the simulations show that a reduction of the barrier layer thickness below 0.5 nm leads to significant tunneling and thus the energy levels decrease and the blue shift is reduced. The matrix solution offers a flexible possibility to handle different potential curves and the numerical solution does not depend on a periodicity of the potential, as it is necessary for the Bloch solution. However, such potential adjustments are not part of the investigations presented here.

### 3. Experimental

The deposition system used for this development was the *Evatec Clusterline 200 BPM* magnetron sputter deposition system, which was discussed in detail in [24–26]. As shown in Fig. 3(a), the system has a turntable and uses a sputter down configuration with a maximum of four magnetron sputter sources (2). For the deposition of  $\text{Ta}_2\text{O}_5$  -  $\text{SiO}_2$  QNL two sputter sources equipped with a silicon and tantalum target respectively were powered simultaneously. The plasma source (3) seen in the foreground is used in standard deposition to influence layer properties such as stress or surface roughness. In the deposition of QNL the plasma source was run optionally since it

enabled operation of the two sources in an even wider parameter range. This tool configuration is shown schematically in Fig. 3(b).

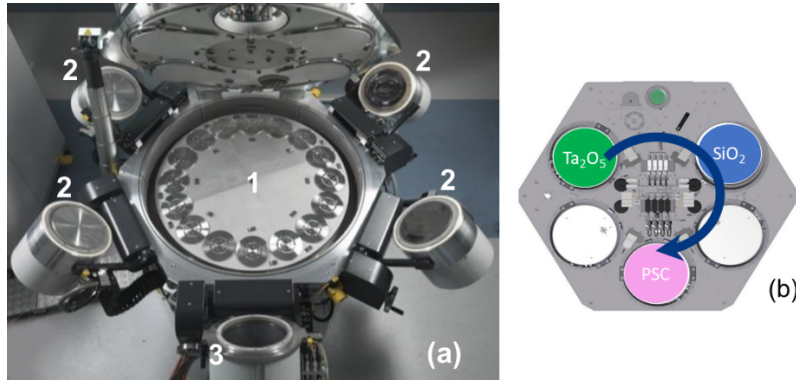


**Fig. 3.** (a): Open Evatec BPME magnetron sputter system: turn table (1), sputter sources (2), plasma source (PSC) (3) in maintenance position. (b) Schematic of sputter process for the QNL layers of Ta<sub>2</sub>O<sub>5</sub> - SiO<sub>2</sub>.

This deposition system has a capacity of 15 substrates of diameter 200 mm. Substrate loading is executed automatically through a load-lock. Oxides are deposited reactively in pulsed DC mode and use plasma emission monitoring (PEM) to exploit the hysteresis effects and assure full oxidation at a high deposition rate. It is also equipped with broad band and monochromatic optical monitoring [27].

The turntable configuration is perfectly suited for the deposition of QNL. With the continuous table rotation substrates pass repeatedly beneath the active tantalum and silicon sources, where sequentially a thin layer of SiO<sub>2</sub> and Ta<sub>2</sub>O<sub>5</sub> is deposited with each rotation. The total thickness deposited in one turn is determined by the rotation speed of the table, a parameter which can easily be varied in a wide range. The thickness ratio of the well and barrier materials is determined by sputter power of the two sources and the related deposition rate. Further deposition parameters, which influence the deposition rate and material properties are the gas flows of argon and oxygen and the PEM set-point. Deposition rates for QNL layers tend to be higher than those for single oxides since they are deposited from two active sources.

The samples were deposited on double side polished fused silica samples. These were characterized by spectrophotometry in transmission and reflection both at an angle of 8° on the exact same spot on the sample by using a *PhotonRT* photospectrometer by *EssentOptics*.

The effective refractive index  $n$  and the extinction coefficient  $k$  in the transparent range of the coating were determined using *OptiChar* by *Optilayer*. The models used were *normal dispersion* for  $n$  and *UV-Vis* mode for the extinction coefficient  $k$ . This evaluation also allows us to determine the physical thickness  $d$  of the metamaterial.

The effective refractive index  $n_{eff}$  is derived from the spectral measurements in T and R as detailed above. The refractive indices of  $n_{high}$  and  $n_{low}$  are derived from Ta<sub>2</sub>O<sub>5</sub> and SiO<sub>2</sub> single layers. The values used were: Ta<sub>2</sub>O<sub>5</sub>  $n_{high} = 2.168$  and SiO<sub>2</sub>  $n_{low} = 1.474$ , both indices relate to a wavelength of 500 nm. Formula (1) then allows us to calculate the volume ratio  $f$  of the two materials.

The thickness per table pass can be calculated by dividing the physical thickness  $d$  of the metamaterial by the number of table passes in the deposition run. The optical band gap was determined using the Tauc-plot method [28].

## 4. Results

### 4.1. Quantum nanolaminate layers of $Ta_2O_5$ - $SiO_2$

In a first experiment, the Si and Ta sources were run at 6 and 5 kW respectively, however with a PEM setting for  $Ta_2O_5$  which resulted in a relatively low deposition rate. The table speed was varied from 3 to 15 seconds per pass, which means that the thickness ratio of high to low layers stayed constant, but the individual layer thickness increased with the slower table speed. The well thickness, i.e. thickness of  $Ta_2O_5$  was determined to be in the range of 0.2-1 nm. According to the theory discussed in section 2, it was expected that the absorption edge would shift towards shorter wavelengths the thinner the individual well layers became, whereas the effective refractive index would remain constant for all five samples. As shown in Fig. 4(a), this behavior was observed in the transmission measurements. The absorption edge of the 3s/pass sample lies at the shortest wavelength, whereas the 15s/pass results in the longest wavelength edge with a difference of 18 nm between the samples. For reference the absorption edge of a  $Ta_2O_5$  layer is indicated by a dotted line. In the longer wavelength range above 280 nm, all curves overlay since they all have the same effective refractive index and optical thickness. Furthermore, they touch the solid line for  $\lambda/2$  optical thickness indicating very low absorption of the QNLs in the longer wavelength range. From these measurements, we can conclude that the magnetron sputtered nanolaminates do show the quantization effect as predicted in [4,5].

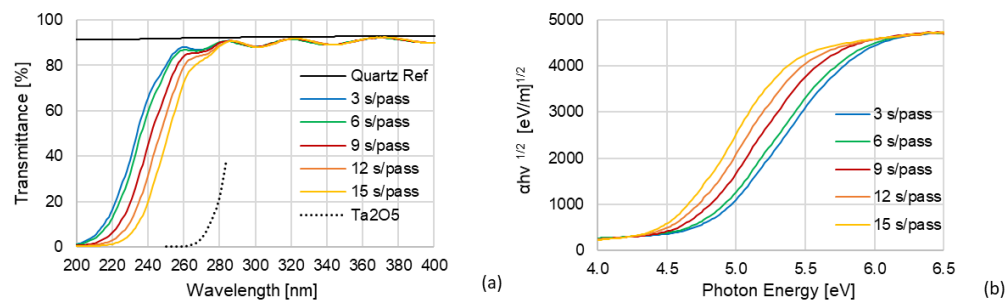


**Fig. 4.** Transmittance (a) and Tauc-plot (b) of QNL layers with the same power ratio of  $Ta_2O_5$  to  $SiO_2$ , but with table speeds (3/6/9/12/15 s/pass).

For this set of samples, the effective refractive index was determined as described in the experimental section. The band gap energy was determined from the Tauc-plot as shown in Fig. 4(b) [29]. The total physical thickness of the QNL layers is in the range of 700 nm, which translates to 600 pairs of nanolaminate layers at a table speed of 3 s/pass.

Figure 5 shows that the gap energy increases with the decrease of well thickness. However, the refractive index remains nearly constant at a value of around 1.56, which corresponds to a thickness ratio of 5.3 of  $SiO_2$  to  $Ta_2O_5$ . Both findings are in perfect agreement with the conclusions, which were already drawn from the observation of the transmission measurements. The shift in absorption edge proves that this stack consists of nanolaminates and is not simply a mixture of both materials. The calculation procedure as mentioned in Section 2 [16] was applied to simulate the gap shift of the deposited QNL coatings, and good agreement between measured energy shifts and the calculation results was found as shown in Fig. 5.

A series of experiments were performed subsequently varying the ratio of the thicknesses of  $Ta_2O_5$  to  $SiO_2$ . The power on each source was varied as a main parameter. Since both sputter processes are PEM-controlled, the PEM settings also had to be adjusted to the values appropriate to the sputter power. With these optimized settings the deposition rates of the nanolaminate layers were higher than for the corresponding single material layers, since nanolaminates are sputtered from two sources.

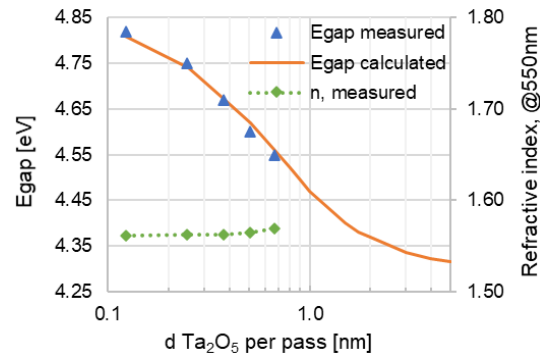


**Fig. 5.** Representation of gap energy and refractive index as a function of the well thickness showing good agreement of the calculated  $E_{\text{gap}}$  compared to the experimental data.

For each H:L ratio a set of deposition runs with different table speeds was completed in order to vary the thickness of the individual nanolaminate layers. Typically, table speeds of 1.5/3/4.5/6/9/12/15 s/pass were chosen. Figure 6(a) shows that the energy of the gap increases as the well thickness gets thinner as also predicted by the theory. For  $\text{Ta}_2\text{O}_5$  with quantum-well thickness exceeding 2–3 nm however, the gap energy becomes constant because thicker layers do not show quantization effects.

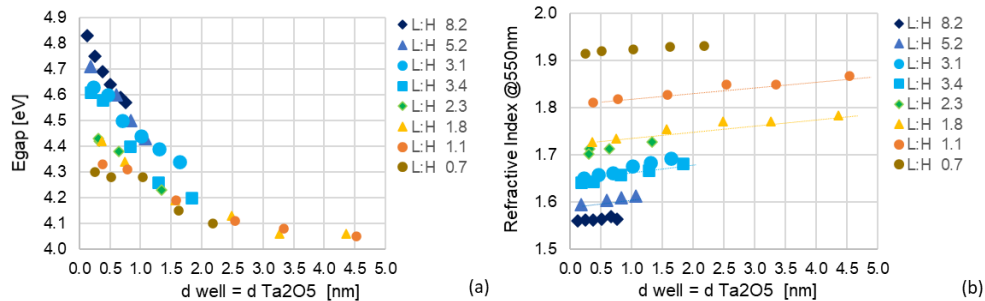


**Fig. 6.** Gap energy and refractive index for a wide range of power ratios. (a) and (b) with relation to the well thickness

On the other hand, the refractive index shows only a slight, but steady increase, with increasing well thickness, the effect being more pronounced the higher the refractive index. As can be seen from Fig. 6(b) the refractive index can be tuned in a very wide range and can basically span a large range between the indices of  $\text{SiO}_2$  to  $\text{Ta}_2\text{O}_5$ .

Figure 7 shows the dependence of band gap energy with refractive index. This representation nicely shows that the band gap energy can indeed be varied for a given refractive index thus decoupling index and gap energy.

#### 4.2. Antireflection coating

The results above demonstrated that magnetron sputter deposition is capable of manufacturing nanolaminates showing the quantum effect. In a next step, we investigated whether optical interference coatings such as antireflection coatings, mirrors or filters could be designed and manufactured by replacing the high refractive material by a QNL stack of the appropriate total thickness.

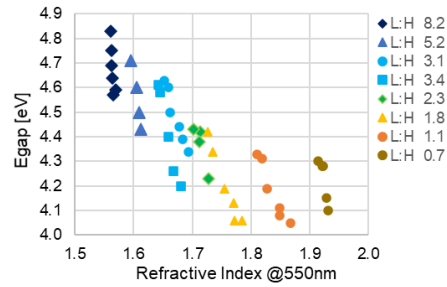


**Fig. 7.** Dependence of gap energy to refractive index.

An antireflection coating for an UV LED centered at 280 nm was chosen as an example for the viability of the QNL concept for optical interference coatings. The design consisted of 2-layers in analogy to a classical V-coating, however with the first layer being a QNL instead of  $\text{Ta}_2\text{O}_5$ . For the experiment, a QNL with an effective refractive index of  $n = 1.7$  at a wavelength of 550 nm and a bandgap energy of  $E_{\text{gap}} = 4.48$  eV was chosen. Such a nanolaminate stack consists of  $\text{Ta}_2\text{O}_5$  and  $\text{SiO}_2$  layers with a thickness of 0.31 and 0.76 nm, respectively. The design uses a thickness of 136 nm for  $\text{SiO}_2$  and a thickness of 120 nm for the QNL, which equals around 120 individual nanolayers of each material. The thicknesses correspond to an optical thickness of around 3 times  $\lambda/4$  at  $\lambda = 280$  nm, which is more than the minimum required  $1 \lambda/4$  to enable an antireflection coating. The thicker layers allowed us to test broad band optical monitoring thickness control in the same experiment.

Figure 8 shows the transmission (a) and reflection (b) measurement curves at  $8^\circ$  angle of incidence of a double side coated quartz substrate. Minimum reflection and maximum transmission occur at the design wavelength of 280 nm and the curves correspond nicely with the design. The transmission of the double side coated sample reaches 98.3% as deposited and 99.2% after annealing for 1 hour at  $300^\circ\text{C}$  in air. The corresponding absorption losses are 1% and 0.3%. In comparison, a 2-layer antireflection coating composed of  $\text{Ta}_2\text{O}_5$  and  $\text{SiO}_2$  optimized for 266 nm resulted in good reflectance at the design wavelength, but 66% and 25% absorption at 266 and 280 nm respectively. This clearly shows that bulk  $\text{Ta}_2\text{O}_5$  cannot be used at these UV-wavelengths, whereas with a QNL consisting of  $\text{Ta}_2\text{O}_5$ - $\text{SiO}_2$  a very good performance can be obtained, enabling to overcome the bandgap limitations of the high refractive index material and opening up the field for a wide range of applications.

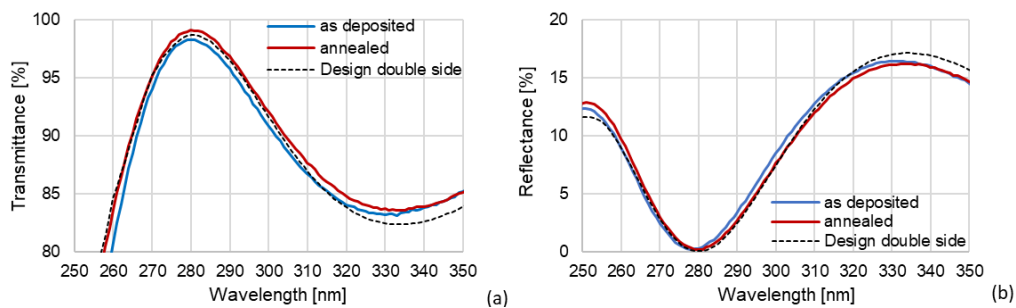


**Fig. 8.** Transmittance (a) and reflectance (b) measurement of the antireflective coating of  $\text{SiO}_2$  and QNL layers showing excellent transmission at 280 nm

In-situ broadband optical monitoring in reflection in a wavelength range of 380-980 nm was used to monitor the coating thickness. Thanks to the thicker layers, the evolution of the signal



could be observed over longer time also through reflection maxima. It turned out, that the reflection signal of the QNL developed in a completely regular way, exactly as a layer with the corresponding effective refractive index would evolve. We can therefore conclude that optical monitoring is perfectly suited for controlling the thickness in film stacks with QNLs in turntable configuration.

#### 4.3. Mirror coating

As a second example of an optical interference coating, a mirror for 355 nm was deposited consisting of 30 layers each of SiO<sub>2</sub> and QNL Ta<sub>2</sub>O<sub>5</sub>-SiO<sub>2</sub> with quarter wave optical thickness. As a comparison, the equivalent mirror with a standard design was deposited with 26 layers total of SiO<sub>2</sub> and Ta<sub>2</sub>O<sub>5</sub> of quarter wave optical thickness.

Both designs were deposited using broadband optical monitoring. The good agreement between measurement and design indicates, that the QNL-layers could be terminated as if they were regular layers, see Fig. 9. Both mirrors are centered nicely at the design wavelength. As expected, the mirror with QNLs has a narrower reflection band due to the lower effective refractive index of the QNL. When comparing the transmission region below the wavelength of 300 nm it becomes obvious, that the standard design only shows poor transmission, whereas the QNL-mirror only has losses in the range of 2-5% above the absorption edge.

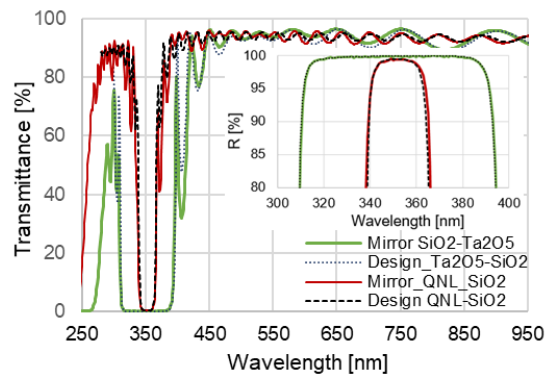


**Fig. 9.** Transmittance and reflectance (inset) measurement at 8° of the mirror for 355 nm comparing a quarter wave design of SiO<sub>2</sub>-QNL with a standard Ta<sub>2</sub>O<sub>5</sub> - SiO<sub>2</sub> coating.

In conclusion, QNL's can be treated in both design and optical monitoring as regular bulk layers with the corresponding effective refractive index. Since two sputter sources are running the deposition rate is also typically higher than for the corresponding single layers of SiO<sub>2</sub> or Ta<sub>2</sub>O<sub>5</sub>.

## 5. Conclusion

In our paper we show that magnetron sputtering using a deposition tool with turntable configuration is ideally suited to depositing quantum nanolaminate layers. The individual layers of the nanolaminate stack are deposited sequentially when passing under the SiO<sub>2</sub> and Ta<sub>2</sub>O<sub>5</sub> sputter sources, a sequence which is repeated with every rotation of the turntable. The setting of the table rotation speed allows to select the total thickness of SiO<sub>2</sub> and Ta<sub>2</sub>O<sub>5</sub> per turn, whereas the power setting of the sources allows to select the thickness ratio of Ta<sub>2</sub>O<sub>5</sub> to SiO<sub>2</sub>. We demonstrated individual layers with a few tenth of nm and a wide range of SiO<sub>2</sub> to Ta<sub>2</sub>O<sub>5</sub> ratios of 0.7-8.

The paper also shows that the predicted shift in the absorption edge is observed. In accordance with theory, the shift becomes larger as Ta<sub>2</sub>O<sub>5</sub> thickness is reduced. The refractive index is given by the ratio of SiO<sub>2</sub> to Ta<sub>2</sub>O<sub>5</sub> layer thicknesses. At a given ratio, the index remains constant or

increases only very slightly when the total thickness of both layers is increased. This finding is also in good agreement with the prediction from theory.

Furthermore, QNL layers were used as the high index material in optical interference filters. We demonstrated that the turntable configuration of the sputter system leads to a viable manufacturing process for an antireflection coating at a wavelength of 280 nm and a mirror at 355 nm. From a technical standpoint the deposition of these filters runs like standard processes with the difference that in the QNL layer both sources are powered. Furthermore, optical monitoring can also be used without any adaptation.

Both antireflection and mirror coatings were in good agreement with the respective designs, and both showed good transmission in the wavelength range below 300 nm where coatings using standard Ta<sub>2</sub>O<sub>5</sub> already operate in their absorptive spectral region. These results confirm that the concept of QNL indeed opens up a wide field for novel applications.

**Funding.** Innosuisse - Schweizerische Agentur für Innovationsförderung (Project 39986.1 IP-ENG); Allianz Industrie Forschung (QuantUV (21364 N)); Deutsche Forschungsgemeinschaft (Cluster of Excellence PhoenixD (390833453, EXC 2122)).

**Acknowledgments.** The authors thank Innosuisse - Swiss Innovation Agency and the Deutsche Forschungsgemeinschaft (DFG, German Research Foundation) for funding under Germany's Excellence Strategy within the Cluster of Excellence PhoenixD (EXC 2122, project ID 390833453).

**Disclosures.** The authors declare no conflicts of interest.

**Data availability.** Data underlying the results presented in this paper are not publicly available at this time but may be obtained from the authors upon reasonable request

## References

1. M. Jupé, T. Willemsen, H. Liu, M. Steinecke, L. Jensen, and D. Ristau, "Manufacturing of Quantized Nanolaminates," in *Optical Interference Coatings 2019, OSA Technical Digest (online)* (Optical Society of America, 2019), paper TB4.
2. T. Willemsen, M. Jupé, L. Gallais, D. Tetzlaff, and D. Ristau, "Tunable optical properties of amorphous Tantalum layers in a quantizing structure," *Opt. Lett.* **42**(21), 4502–4505 (2017).
3. H. Finkenrath, "The moss rule and the influence of doping on the optical dielectric constant of semiconductors-i," *Infrared Phys.* **28**(5), 327–332 (1988).
4. H. Badorreck, M. Steinecke, L. Jensen, D. Ristau, M. Jupé, J. Müller, R. Tonneau, P. Moskovkin, S. Lucas, A. Pflug, L. Grinevičiūtė, A. Selskis, and T. Tolenis, "Correlation of structural and optical properties using virtual materials analysis," *Opt. Express* **27**(16), 22209 (2019).
5. T. Tolenis, L. Grinevičiūtė, R. Buzelis, L. Smalakys, E. Pupka, S. Melnikas, A. Selskis, R. Drazdys, and A. Melninkaitis, "Sculptured anti-reflection coatings for high power lasers," *Opt. Mater. Express* **7**(4), 1249–1258 (2017).
6. L. Grinevičiūtė, M. Andrulevicius, A. Melninkaitis, R. Buzelis, A. Selskis, A. Lazauskas, and T. Tolenis, "Highly Resistant Zero-Order Waveplates Based on All-Silica Multilayer Coatings," *Phys. Status Solidi A* **214**(12), 1700764 (2017).
7. T. Tolenis, L. Grinevičiūtė, L. Smalakys, M. Šciuka, R. Drazdys, L. Mažule, R. Buzelis, and A. Melninkaitis, "Next generation highly resistant mirrors featuring all-silica layers," *Sci. Rep.* **7**(1), 10898 (2017).
8. R. Tonneau, P. Moskovkin, A. Pflug, and S. Lucas, "TiO<sub>x</sub> deposited by magnetron sputtering: a joint modelling and experimental study," *J. Phys. D: Appl. Phys.* **51**(19), 195202 (2018).
9. R. Tonneau, P. Moskovkin, J. Muller, T. Melzig, E. Haye, S. Konstantinidis, A. Pflug, and S. Lucas, "Understanding the role of energetic particles during the growth of TiO<sub>2</sub> thin films by reactive magnetron sputtering through multi-scale Monte Carlo simulations and experimental deposition," *J. Phys. D: Appl. Phys.* **54**(15), 155203 (2021).
10. U. Schulz, "Review of modern techniques to generate antireflective properties on thermoplastic polymers," *Appl. Opt.* **45**(7), 1608–1618 (2006).
11. U. Schulz, B. Schallenberg, and N. Kaiser, "Symmetrical periods in antireflective coatings for plastic optics," *Appl. Opt.* **42**(7), 1346–1351 (2003).
12. U. Schulz, F. Rickelt, P. Munzert, and N. Kaiser, "A double nanostructure for wide-angle antireflection on optical polymers," *Opt. Mater. Express* **4**(3), 568–574 (2014).
13. J. Dervaux, P.-A. Cormier, P. Moskovkin, O. Douheret, S. Konstantinidis, R. Lazzaroni, S. Lucas, and R. Snyders, "Synthesis of nanostructured Ti thin films by combining glancing angle deposition and magnetron sputtering: A joint experimental and modeling study," *Thin Solid Films* **636**, 644–657 (2017).
14. T. Willemsen, M. Jupé, M. Gyamfi, S. Schlichting, and D. Ristau, "Enhancement of the damage resistance of ultra-fast optics by novel design approaches," *Opt. Express* **25**(25), 31948–31959 (2017).
15. M. Steinecke, H. Badorreck, M. Jupé, T. Willemsen, L. Hao, L. Jensen, and D. Ristau, "Quantizing nanolaminates as versatile materials for optical interference coatings," *Appl. Opt.* **59**(5), A236–A241 (2020).

16. T. Willemsen, P. Geerke, M. Jupe, L. Gallais, and D. Ristau, "Electronic quantization in dielectric nanolaminates," *Proc. SPIE* **10014**, 100140C (2016).
17. P. Harrison and A. Valavanis, "*Quantum Wells, Wires and Dots: Theoretical and Computational Physics of Semiconductor Nanostructures*", 4th Edition (Wiley, 2016).
18. C. Franke, O. Stenzel, S. Wilbrandt, J. Wolf, N. Kaiser, and A. Tünnermann, "Estimation of the composition of coelectron-beam-evaporated thin-mixture films by making use of the Wiener bounds," *Appl. Opt.* **54**(9), 2362–2370 (2015).
19. R. Jansson and H. Arwin, "Selection of the physically correct solution in the n-media Bruggeman effective medium approximation," *Opt. Commun.* **106**(4-6), 133–138 (1994).
20. A. Feldman, "Modeling refractive index in mixed component systems," in *Modeling of Optical Thin Films*, Vol. 0821, (1988).
21. T. Amotchkina, D. Ristau, M. Lappschies, M. Jupe, A. Tikhonravov, and M. Trubetskov, "Optical Properties of TiO<sub>2</sub>-SiO<sub>2</sub> Mixture Thin Films Produced by Ion-Beam Sputtering," in *Optical Interference Coatings (OIC) 2007, OSA Technical Digest* (Optica Publishing Group, 2007), paper TuA.8.
22. "MedeA," <https://www.materialsdesign.com/medea-software>.
23. M. Turowski, T. Amotchkina, H. Ehlers, M. Jupé, and D. Ristau, "Calculation of optical and electronic properties of modeled titanium dioxide films of different densities," *Appl. Opt.* **53**(4), A159–A168 (2014).
24. S. Schwyn Thöny, M. Chesaux, S. Gees, and A. Frigg, "Innovative sputter system for high volume production of demanding optical interference coatings," in *Optical Interference Coatings 2016, OSA Technical Digest (online)* (Optical Society of America, 2016), paper WA.7.
25. M. Chesaux, S. Schwyn Thöny, S. Gees, and A. Frigg, "Rotating target source: novel shaperless concept for magnetron sputtering with excellent uniformity," in *Optical Interference Coatings 2016, OSA Technical Digest (online)* (Optical Society of America, 2016), paper WA.2.
26. S. Schwyn Thöny, S. Gees, and E. Schüngel, "Improving film stress and surface roughness by using a plasma source in magnetron sputtering," in *Optical Interference Coatings 2019, OSA Technical Digest (online)* (Optical Society of America, 2019), paper WC.4.
27. S. Waldner, J. Buchholz, and R. Benz, "Hybrid Mode Optical Monitoring – Monochromatic and Broadband Algorithms in the same Coating Process," in *Optical Interference Coatings Conference (OIC) 2019, OSA Technical Digest* (Optica Publishing Group, 2019), paper WA.9.
28. B. D. Vierzicke, S. Patel, B. E. Davis, and D. P. Birnie, "Evaluation of the tauc method for optical absorption edge determination: ZnO thin films as a model system," *Phys. Status Solidi B* **252**(8), 1700–1710 (2015).
29. O. Stenzel, "*The physics of thin film optical spectra*", Berlin/Heidelberg, Germany (Springer, 2015).